Journal of Sound and Vibration (2000) **238**(4), 595–615
doi:10.1006/jsvi.2000.3106, available online at http://www.idealibrary.com on IDEAL®

INFLUENCE OF BALLAST ON WAVE STEEPENING IN TUNNELS

A. E. Vardy and J. M. B. Brown

*Civil Engineering Department, University of Dundee, Dundee DD*1 4*HN, Scotland*

(*Received* 4 *August* 1999, *and in final form* 26 *April* 2000)

The strength of micro-pressure waves emitted from railway tunnels is strongly dependent upon the steepnesses of wavefronts arriving at tunnel portals after travelling along the tunnel. The steepnesses are themselves dependent upon the ability of phenomena such as skin friction to resist inertial steepening. In this paper, the influence of air pockets in ballast track is investigated. First, the local behaviour of the ballast is linked to a series of Helmholtz resonators, yielding analytical relationships whose characteristics are explored. Then the resonators are incorporated into a simple model of wave propagation in ducts. By initially neglecting skin friction, the existence of stable, asymptotic conditions is identified. The asymptotes are shown to depend upon the pressure amplitude but to be independent of the upstream rates of change of pressure. The consequences of these results in real tunnels are illustrated.

1. INTRODUCTION

The magnitudes of pressure waves generated by railway trains entering tunnels vary approximately with the square of the train speed. To protect passengers from exposure to large changes, it is increasingly common for modern high-speed trains to be partially sealed aerodynamically. The cost of sealing is more acceptable than, say, the cost of building larger-diameter tunnels or temporarily reducing speeds during tunnel entry and exit.

The sealing of trains does not, however, mitigate a second consequence of the pressure waves, namely the emission of so-called *micro-pressure waves* from tunnel portals. In many tunnels, these are little more than low-frequency noise of small amplitude. In severe cases, however, the result can resemble a loud crack that sounds like a sonic boom. The disturbance, which can shake doors and windows of nearby buildings, has been a source of practical concern in Japan for some decades [1, 2] and it is now attracting attention from European rail operators [3].

The amplitudes of the micro-pressure waves are dependent upon the frequency distributions of compression wavefronts arriving at the tunnel exit portal. In most tunnels, however, the amplitudes correlate closely with a single parameter, namely the maximum rate of change of pressure in the incident wavefront [4]. This is because wavefronts tend to have a common characteristic shape after propagating sufficiently far along a tunnel. In practice, the correlation works quite well even when comparing different tunnels. That is, the most important property of wavefronts arriving at exit portals is their maximum rate of change of pressure, not their absolute amplitude.

Many methods of reducing the strengths of the micro-pressure waves are possible. Some of these attack the reflection process directly through passive or active devices at the tunnel exit [5–8]. Others seek to prevent the arrival of steep wavefronts along the tunnel. They

0022-460X/00/490595 + 21 $35.00/0

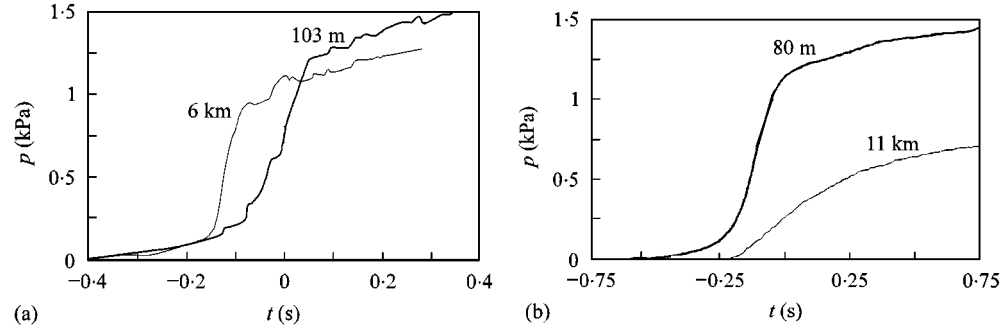

Figure 1. Wavefront propagation in a railway tunnel (after Mashimo *et al.* [15]). Relative times of graphs are indicative only. (a) Slab track; (b) ballast track.

either reduce the steepness of the wavefront generated during train-entry [9, 10] or disrupt the inertial steepening process as the wavefront propagates along the tunnel [11, 12].

1.1. WAVEFRONT PROPAGATION

The generation of the wavefront during train-entry [13] and the radiation of the micro-pressure waves at the tunnel exit [14] can be simulated numerically with good accuracy. Both events are inertia-driven, at least to first order. In contrast, the evolution of the pressure distribution local to the wavefront as it propagates along the tunnel is less well predicted. It is strongly influenced by dissipative phenomena as well as by inertia.

Consider the simple case of a wavefront propagating along a tunnel with smooth concrete surfaces. The track and other fixtures in the tunnel cause some large-scale roughness, but the overall geometry is simple. Mashimo *et al.* [15] report measurements in such a tunnel in Japan. Figure 1(a) shows the measured pressure approximately 100 m from the tunnel entrance portal together with the corresponding event after the wavefront has travelled about 6 km. The relative positions of the two curves on the time axis have been chosen by the present authors to convey the general message that the leading edge of the wavefront steepens, but that the overall amplitude has reduced. Fukuda *et al.* [16] showed that this behaviour can be attributed to skin friction forces exhibiting both quasi-steady and unsteady behaviour.

Figure 1(b) shows corresponding pressure histories presented by Mashimo *et al.* [15] for a tunnel with a ballast track. Once again, the relative positions on the time axis have been chosen by the present authors, showing that the wavefront has flattened and that the overall amplitude has reduced greatly. On arrival at the tunnel exit portal, the wavefront is far less steep than in the slab-track case, thereby explaining why ballast-track tunnels do not usually give rise to unacceptable micro-pressure waves. It would clearly be useful to be able to reproduce this behaviour in a reliable manner in order to assess in advance which tunnels might require portal modifications and which will not.

1.2. OUTLINE OF PAPER

The first purpose of this paper is to present a method of analyzing the propagation of wavefronts along ballast–track tunnels. A second purpose is to explain the underlying

physical behaviour and to show that ballast can have a dominant influence even in relatively short tunnels. The development begins in section 2 with a description of the mathematical model used to represent air flows in the ballast. The response of the ballast air to prescribed pressure histories in the air just above the track is then investigated to enable characteristic time scales to be found. These are used to guide the inclusion of a theoretical model of the ballast behaviour in a simulation of plane pressure wave propagation along a tunnel. A range of values of the ballast properties and dimensions is investigated in section 3 to assist in understanding behaviour in real tunnels.

In the main body of the paper, no account is taken of skin friction. This simplification is adopted partly for simplicity, but mostly to allow the effect of the air space in the ballast to be studied as a separate entity. It has a valuable payoff in section 3 where the existence of an asymptotic behaviour is identified. The asymptotic condition is an important factor in understanding why incident wavefronts at tunnel portals tend to have characteristically similar shapes.

2. LOCAL BEHAVIOUR OF BALLAST

2.1. BALLAST PROPERTIES

Much existing railway track is laid on a ballast bed comprising, say, 500 mm depth of angular stones. The bed is compacted before tracks are laid so that trains will not cause undue settlement. Typically, the individual stones for main-line track are in the order of 30–60 mm and the porosity of new ballast (i.e., volume of voids ÷ total volume) is about 0·40.

Suppose that a ballast bed is 8 m wide and 0·5 m deep. If the porosity is 0·4, then the total volume of included air per metre length of tunnel is about 1·6 m^3. Typically, this is between 2 and 3% of the free-space volume of air above the ballast. There is therefore little scope for the ballast to have a substantial influence on absolute pressures in the tunnel. Nevertheless, it can have a strong influence on rapid rates of change of pressure.

The influence of the ballast depends not only on the total volume (or mass) of air available for compression, but also on the times required for the pressurization and de-pressurization processes to occur. These, in turn, depend primarily upon two factors, namely (1) the resistance to quasi-steady flows in the ballast and (2) inertial forces associated with changes to rates of flow.

In effect, the ballast acts as a porous acoustic liner and its characteristic response is determined primarily by its acoustic impedance [17, 18]. Ozawa *et al.* [19] recognized that the impedance could be modelled by regarding the ballast as analogous to an array of Helmholtz resonators. They followed an approach used by Morse [18] to develop expressions for lumped parameters representing the acoustic impedances of porous liners. They assumed that the influence of airflows in the plane of the ballast may be neglected in comparison with flows normal to the plane, although it was later found that these can have a small influence [4].

2.1.1. *Compliance*

Using the analogy shown schematically in Figure 2, the volume of entrapped air in a vertical column of ballast of unit surface area, depth h and porosity e is eh. Thus, the compliance C per unit surface area of ballast is

$$C = \frac{(\gamma)eh}{\rho c^2}, \tag{1}$$

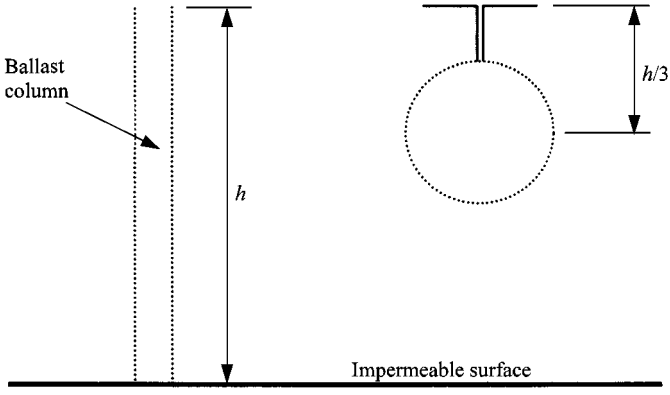

Figure 2. Representation of ballast as a Helmholtz resonator.

in which γ is the ratio of the principal specific heat capacities of the air, ρ is the density of air and c is the local speed of sound. The compliance may be interpreted as a specific acoustic impedance coefficient. The greater its value, the greater the potential for pressure reduction, both overall and close to wavefronts.

The inclusion of γ in equation (1) implies the existence of isothermal conditions within the ballast. This is reasonable at low frequencies, but at sufficiently high frequencies, it would be more plausible to assume adiabatic conditions and hence to omit γ.

2.1.2. *Resistance*

If air flowed steadily in only one direction through a sample of ballast, the pressure would decrease in the direction of flow. The pressure gradient at any particular flow rate would be a measure of the resistance of the medium. For a porous medium, the resistivity r is defined as the ratio of the pressure gradient $\partial p/\partial z$ in the direction of flow and the velocity w (based on the full area, not on the pore area), i.e.,

$$r \equiv \frac{|\partial p/\partial z|}{w}. \tag{2}$$

The resistivity may be regarded as a resistance per unit area and per unit length in the direction of flow. For practical usage, it is desirable to introduce a bulk resistance of the whole depth of ballast. Consider vertical flow between the overlying air and the included air. The velocity will vary from a maximum of w_0 at the surface to zero at the bed whereas a single parameter resistance must be based on a single velocity, herein chosen as w_0. Following Morse [18, p. 365] the resistance per unit area, R, is taken as

$$R = \frac{rh}{3}, \tag{3}$$

in which the factor of 3 allows for the vertical distribution of velocity.

2.1.3. *Inertance*

The inertance H of the column per unit surface area of ballast is

$$H = \frac{\xi \rho h/3}{e}, \tag{4}$$

in which the factor of 3 again allows for the vertical distribution of velocity [18]. The empirical parameter ξ allows, for example, for apparent mass effects because of non-uniform velocity distributions in the tortuous flow paths through the pore structure.

2.1.4. *Non-uniform ballast*

The above expressions are applicable to a homogeneous ballast of the sort that might be achieved in laboratory tests. In a real tunnel, however, the ballast can vary strongly with depth. It is reasonable to expect, for instance, that ballast near the bed will be more highly compacted than that near the surface. Also, small particles will tend to migrate towards the bottom and allowance should be made for factors such as surface caking and moisture ingress. These differences from an ideal geometry are important because the resistivity of a porous medium depends very strongly on its porosity (sometimes to the fourth or fifth power). To allow for this effect, the real ballast is imagined herein to be replaced by a uniform ballast with a much greater *effective* resistivity than the ideal ballast. They are much greater than values obtained by Ozawa [19] in laboratory tests, but much smaller than values obtained by Embleton *et al.* [20] for sound wave reflections over gravel surfaces in the open.

2.2. EQUATION OF FLOW IN THE BALLAST

Using the lumped parameters defined above, the equation of motion for the air in the stem of the equivalent resonator can be expressed as

$$H\frac{\mathrm{d}^2\zeta_0}{\mathrm{d}t^2} + R\frac{\mathrm{d}\zeta_0}{\mathrm{d}t} + \frac{1}{C}\zeta_0 = p(t), \tag{5}$$

where ζ_0 is the displacement of the air at the neck and $p(t)$, the forcing pressure at the neck, is a prescribed function of time.

Alternatively, using the velocity at the neck, namely

$$w_0 = \mathrm{d}\zeta_0/\mathrm{d}t, \tag{6}$$

equation (5) may be written as

$$H\frac{\mathrm{d}w_0}{\mathrm{d}t} + Rw_0 + (1/C)\int_0^t w_0\,\mathrm{d}t = p(t). \tag{7}$$

On the assumption that the air is initially at rest, the Laplace transform of equation (7) leads, after some rearrangement, to

$$w_0'(s) = \left[\frac{1}{H}\right]\left[\frac{1}{(s+\alpha)^2 + \{\omega_n^2 - \alpha^2\}}\right][sp'(s)], \tag{8}$$

where s is the Laplace transform parameter, $w_0'(s)$ and $p'(s)$ are the Laplace transforms of $w_0(t)$ and $p(t)$, respectively, α is a damping factor defined by equation (9) and ω_n is a natural

frequency defined by equation (10):

$$\alpha \equiv R/2H, \tag{9}$$

$$\omega_n^2 \equiv 1/HC. \tag{10}$$

The inverse Laplace transform of equation (8) can be expressed as a convolution, namely

$$w_0(T) = \left[\frac{1}{H}\right] \int_0^{T^*} \frac{\partial p}{\partial t}(t)\,[W(t^*)]\,\mathrm{d}t^*, \tag{11}$$

where T is the current time, $t^* = T - t$ is a backward measured time, $T^* \leqslant T$ is the time for which the integral makes a significant contribution and W is a weighting function satisfying

$$W(t^*) = \mathscr{L}^{-1}\left\{\frac{1}{[s+\alpha]^2 + [\omega_n^2 - \alpha^2]}\right\}(t^*), \tag{12}$$

in which $\mathscr{L}$ is the Laplace transform operator.

2.3. SUBCRITICAL, CRITICAL AND SUPERCRITICAL DAMPING

The nature of the weighting function is dependent upon the relative magnitudes of the damping factor α and the undamped natural frequency ω_n. The cases of subcritical, critical and supercritical damping, respectively, are given by

(a) When $\alpha < \omega_n$,

$$W(t^*) = \exp[-\alpha t^*]\,\frac{\sin[t^*\sqrt{\omega_n^2 - \alpha^2}]}{\sqrt{\omega_n^2 - \alpha^2}}. \tag{13}$$

(b) When $\alpha = \omega_n$,

$$W(t^*) = t^* \exp[-\alpha t^*]. \tag{14}$$

(c) When $\alpha > \omega_n$,

$$W(t^*) = \exp[-\alpha t^*]\,\frac{\sinh[t^*\sqrt{\alpha^2 - \omega_n^2}]}{\sqrt{\alpha^2 - \omega_n^2}} \tag{15}$$

and the corresponding behaviours are illustrated in Figure 3.

The case of critical damping ($\alpha = \omega_n$) merits attention because it enables the likely conditions in any particular tunnel to be assessed. For given numerical values of (1) compliance per unit depth, (2) resistivity and (3) inertance per unit depth, there exists a particular depth of ballast for which $\alpha = \omega_n$, namely

$$h_{crit} = [\rho c/re]\,\sqrt{12\xi/\gamma}. \tag{16}$$

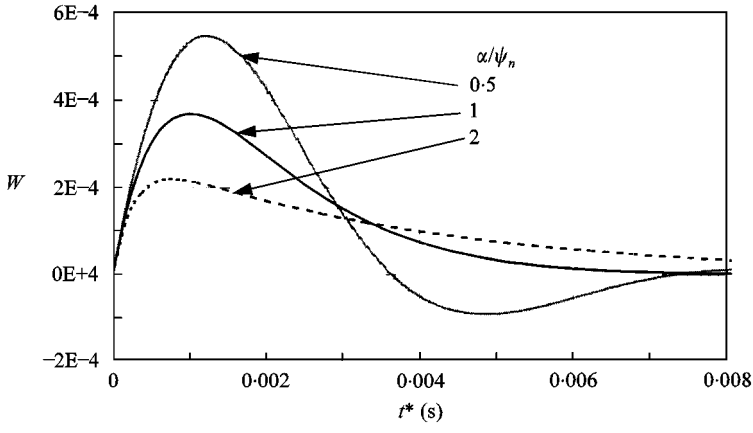

Figure 3. Typical weighting functions for sub-critical ($\alpha/\omega_n = 0{\cdot}5$), critical ($\alpha/\omega_n = 1{\cdot}0$) and super-critical ($\alpha/\omega_n = 2{\cdot}0$) damping.

As an example, a ballast of porosity $e = 0{\cdot}4$ and effective resistivity $r = 10^{4{\cdot}5}$ Pa s/m^2 has a critical depth of approximately 0·10 m. If the actual ballast depth is smaller than this, the response to a step change in the impressed pressure will be oscillatory. If the actual depth is greater than h_{crit}, the response will be monotonic.

The remainder of this paper is applicable only to ballast exhibiting supercritical damping. This contracts with Ozawa *et al.* [4, 19], whose analysis corresponds to the use of equation (13), thereby implying subcritical damping. Their resistivities were based on samples of ballast formed in a laboratory environment.

2.4. CONSTANT RATE OF CHANGE OF PRESSURE

Useful indicative information about physical timescales can be obtained by considering the special case of a constant rate of change of the impressed pressure. Assuming supercritical damping and using $\dot{P}$ to denote the constant rate of change of pressure, equation (11) can be integrated to give

$$w_0 = \frac{\dot{P}}{2\beta H}\left[\frac{1}{\alpha-\beta} - \frac{1}{\alpha+\beta} - \left\{\frac{e^{[-\{\alpha-\beta\}T^*]}}{\alpha-\beta} - \frac{e^{[-\{\alpha+\beta\}T^*]}}{\alpha+\beta}\right\}\right], \tag{17}$$

where the parameter β, introduced for clarity, is defined by

$$\beta \equiv \sqrt{\alpha^2 - \omega_n^2}\,. \tag{18}$$

As T^* increases, the exponential terms in equation (17) tend to zero. The remaining terms may therefore be interpreted as a limiting velocity, which, using equation (10) and (18), can be expressed as

$$w_{0\infty} = \dot{P}C. \tag{19}$$

Using equation (1), this becomes

$$w_{0\infty} = \frac{(\gamma)ehP}{\rho c^2}, \tag{20}$$

which is independent of the resistivity of the ballast. As an example, with a ballast for which $e = 0{\cdot}4$ and $h = 0{\cdot}5$ m, a sustained pressure increase of 10 kPa/s would induce a limiting velocity of about 0·02 m/s.

To estimate the time required to approach the limiting velocity, consider the four terms in square brackets in equation (17). When α is much greater than ω_n, $(\alpha - \beta)$ is much smaller than $(\alpha + \beta)$ and so the second and fourth terms are small in comparison with the first and third terms respectively. Now consider only the latter pair and note that the influence of the exponential term reduces as the limiting velocity is approached. The time required to reach, say, 98% of the limiting velocity corresponds to the time when the exponential term has reduced to 2% of the first term and so

$$T_L^* = \frac{-\ln 0{\cdot}02}{\alpha - \beta}. \tag{21}$$

With an effective resistivity of $r = 10^{4{\cdot}5}$ Pa s/m^2, the above ballast yields $\alpha \approx 5270\ \mathrm{s}^{-1}$ and $\alpha - \beta \approx 95\ \mathrm{s}^{-1}$ and so the limiting time is $T_L^* \approx 41{\cdot}2$ ms. With an effective resistivity of 10^4 Pa s/m^2, the corresponding time is 11·9 ms. Thus, although the limiting value of the inflow velocity is independent of the resistivity, the time to attain this value is strongly influenced by resistivity. The potential influence on wavefront shapes can be inferred by noting that the above times are sufficient for a wavefront to propagate about 10·7 and 3·1 m respectively along a tunnel.

2.4.1. *Ramp pressure change*

As a first approximation, a pressure wavefront propagating along a tunnel may be considered as a linear increase in pressure from zero to a constant value. In Figure 4(a), the ramp is labelled "ramp 1" and the constant pressure zone is regarded as the superposition of this ramp with an equal and opposite "ramp 2". Figure 4(b) shows the predicted surface velocity w_0 for the combined ramps for a particular ballast.

The first ramp causes a gradual increase in w_0 which closely approaches its limiting value before the second ramp begins. Thereafter, the velocity decreases in a mirror-image manner. The area under the curve is a measure of the amount of air that enters a unit surface area of the ballast during the passage of the ramp.

2.5. FINITE-DIFFERENCE FORM OF THE BALLAST SURFACE VELOCITY INTEGRAL

In section 3, the equations describing the behaviour of the ballast are solved simultaneously with equations describing longitudinal wave propagation along the tunnel. To simplify this process, the ballast equation is developed into a form suitable for numerical integration. The backward time T^* is divided into n equal intervals Δt^*, which are assumed to be sufficiently small for W and $\partial p/\partial t$ to be regarded as approximately constant in any interval. Equation (11) is thus approximated by

$$w_0(T^*) \approx \frac{3e}{\xi \rho h} \sum_{k=1}^{n} W(t_k^*)\, \Delta p_k, \tag{22}$$

where $W(t_k^*)$ is the value of the weighting function at the mid-point of the kth backward time interval and Δp_k is the pressure change during that interval.

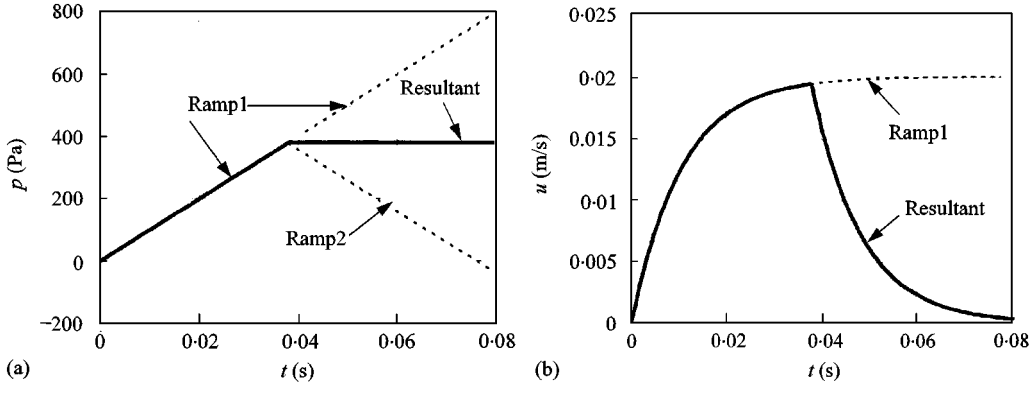

Figure 4. Response of ballast surface velocity to impressed pressure change. ($h = 0{\cdot}5$ m, $e = 0{\cdot}4$, $r = 10^{4{\cdot}5}$ Pa s/m^2). (a) prescribed pressure; (b) induced velocity.

In the numerical implementation, the time steps of the calculation process must be sufficiently small to ensure that this approximation is adequate. This implies the use of smaller grid sizes than are usual in analyses of one-dimensional plane waves.

3. LONGITUDINAL WAVE PROPAGATION

The preceding development deals with the response of ballast to impressed pressure changes. Attention now turns to the analysis of the longitudinal waves that cause the changes. In the numerical model adopted herein, the ballast is regarded as being concentrated in discrete pockets at grid points in the numerical scheme used to analyze the wave propagation (see Figure 5). The pressures just upstream (A) and downstream (B) of a typical grid point are equal, but the velocities differ because of flow into and out of the ballast. The (inviscid) wave propagation between grid points is purely inertial.

This form of discretization is loosely analogous to that used by Wylie and Streeter [21] to model wave propagation in cavitating liquid flows. Waves propagating along the typical paths LA and RB in Figure 5 arrive simultaneously at the double-grid point A, B at the time $t_2 = t_1 + \Delta t$. At this grid point, four equations are needed in four unknowns: u_A is the axial velocity to the left of the grid point; u_B is the axial velocity to the right of the grid point; w_0 is the lateral velocity across the surface of the ballast; and p is the pressure at the grid point.

There are two wave equations, a continuity equation and a ballast equation (22). In equation (22), the term denoted by $k = 1$ involves the pressure p at the solution time whereas all remaining terms (i.e., $k > 1$) can be evaluated explicitly from historical data in the time-marching numerical process.

The wave equations, expressed in characteristics form using a homentropic approach justified by Benson and Ucer [22] for flows with low friction and Mach number, lead to

$$\frac{2}{\gamma - 1}(c_A - c_L) + (u_A - u_L) = 0 \tag{23}$$

and

$$\frac{2}{\gamma - 1}(c_B - c_R) - (u_B - u_R) = 0, \tag{24}$$

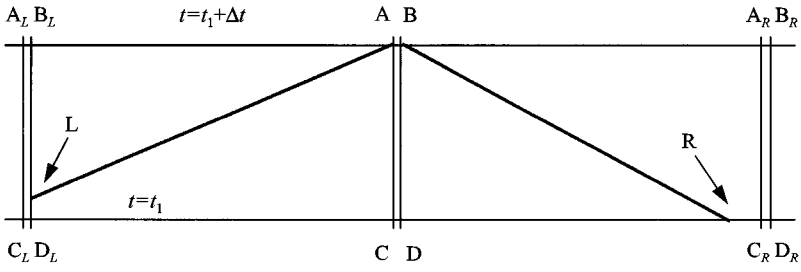

Figure 5. Double-valued grid points in a fixed grid for wave propagation.

in which the speed of sound c is related to the pressure p by

$$\frac{p}{p_\infty} = \left\{\frac{c}{c_\infty}\right\}^{2\gamma/(\gamma-1)}. \tag{25}$$

where p_∞ and c_∞ are reference values.

The continuity equation is

$$u_A a = u_B a + w_0 b \Delta x, \tag{26}$$

where a is cross-sectional area of the tunnel, b is the width of the ballast across the tunnel, and Δx is the distance between successive grid points.

The set of equations is solved iteratively to provide the values of the three velocities and the pressure (and hence the sound speed) at the typical double points A and B.

3.1. SOLUTION SEQUENCE

The initial condition throughout the tunnel is zero flow and uniform pressure. This condition is disturbed by prescribing a pressure history at the left-hand boundary, causing a compressive wavefront to travel from left to right along the tunnel. At each solution instant, the overall solution sequence is from left to right in Figure 5. That is, the conditions are determined first at the left hand (upstream) boundary, then at the nearest grid point, then at the next grid point, etc. This sequence enables advantage to be taken of the known direction of wave propagation.

Before equations (23) and (24) can be used, it is necessary to deduce numerical values for the parameters c and u at the points L and R. At the point R, the values are obtained by interpolation between the points D and D_R at the earlier solution time. At the point L, the interpolation is between the points D_L and B_L. The latter is available explicitly because of the use of the left-to-right sweep in the solution sequence.

The use of interpolation is inherently undesirable, especially in analyses of wavefront development, because the fixed-grid method of characteristics is not conservative. Ideally, a natural characteristics grid should be used, but this is not practical here because it conflicts with the need to obtain pressures at fixed locations along the tunnel (i.e., at the Helmholtz resonators). The adverse consequences of interpolation are minimized in the following ways:

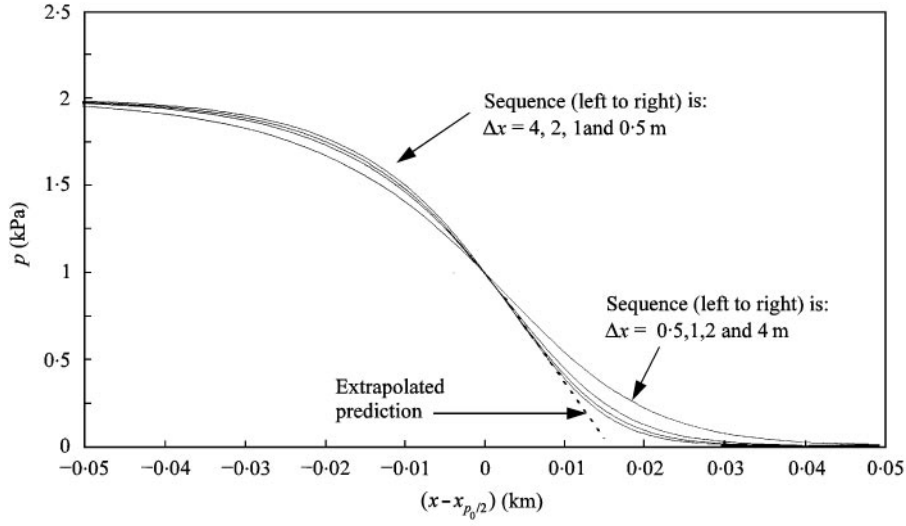

Figure 6. Influence of numerical grid size on predicted wavefront shape ($b = 8$ m, $h = 0{\cdot}5$ m, $e = 0{\cdot}4$, $r = 10^{4{\cdot}5}$ Pa s/m^2).

(1) Solutions are obtained and compared for successively smaller grid sizes (see section 3.2);
(2) The *shape* of the numerical grid (i.e., the ratio $\Delta x/\Delta t$) is chosen to ensure that the mid-pressure position of the wavefront is uninfluenced by interpolation. This is done by selecting the increment Δt at each solution time to ensure that $\Delta x/\Delta t$ is equal to the value of $u + c$ at the position on the wavefront where $p = p_0/2$.

3.2. GRID SIZE DEPENDENCE

Figure 6 illustrates the influence of the grid size on a typical prediction of a wavefront shape after it has travelled several kilometres along a ballast track tunnel with a cross-sectional area of 60 m^2. For clarity, the curves are aligned relative to their mid-pressure positions. By inspection, the solution has almost converged with a grid size of 1 m. Successive reductions by a factor of 2 in the grid size have strongly decreasing influence of the predicted maximum pressure gradient (the key parameter for design purposes). This is further illustrated in Figure 7 which shows the grid size dependence of the maximum pressure gradients after the wavefront has travelled for 10 and 20 s.

In Figure 6, the grid-size dependence is less strong in the high-pressure region than in the low-pressure region at the leading toe of the wavefront. As the grid size is reduced, the leading part of the wavefront approaches more closely to the hand-drawn curve labelled "extrapolated prediction". Results not presented here have confirmed that the true curve should be close to this line. They have been obtained using very small grid sizes and alternative methods of choosing calculation time steps.

Notwithstanding the separate tests, the results presented in the remainder of this paper have been obtained using the numerical scheme leading to the curve labelled $\Delta x = 1$ m in Figure 6. This is regarded as a reasonable compromise between conflicting needs for high accuracy and acceptable CPU times. In all subsequent figures, the influence of grid size can be assessed by observing the extent of the dissipation at the toe of the wavefront. The true curves should be assumed to have the general shape indicated by the hand-drawn extrapolation in Figure 6.

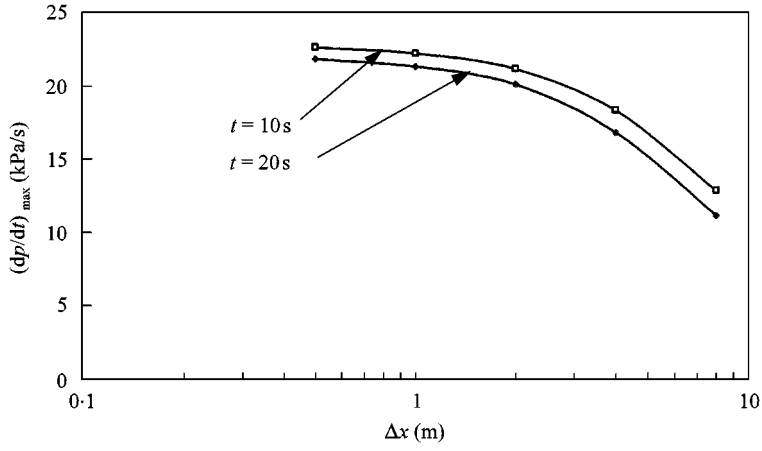

Figure 7. Influence of numerical grid size on predicted maximum rates of change of pressure ($p_0 = 2$ kPa, $b = 8$ m, $h = 0{\cdot}5$ m, $e = 0{\cdot}4$, $r = 10^{4{\cdot}5}$ Pa s/m^2).

3.3. ECONOMIC PROCEDURE FOR LONG TUNNEL CALCULATIONS

The need for fine detail in the numerical simulations leads to unusually large CPU times for one dimensional analyses. These are caused partly by the very long tunnels to be simulated, partly by the use of exceptionally small grid sizes and partly by nested iterative loops that are needed to avoid even stronger grid-size dependence. As an example, consider the use of a grid size of $\Delta x = 1$ m in a tunnel of length $L = 10$ km. This implies a need for 10 000 grid points, at each of which calculations must be undertaken at 10 000 time steps.

This process is shortened here by regarding the 10 km tunnel as a series of, say, 10 1 km tunnels, each of which is much longer than the length of the significant part of the wavefront. The predicted pressure–velocity history at a suitable location upstream of the right-hand end of each tunnel is used as the prescribed boundary condition at the left-hand end of the next tunnel. This greatly reduces the number of superfluous calculations far ahead of the wavefront and far behind it. The necessary CPU time reduces approximately in proportion to the number of tunnel segments.

4. EVOLUTION OF WAVEFRONTS

4.1. STEP WAVEFRONT

Figure 8 shows successive pressure distributions as a wavefront propagates along a 60 m^2 tunnel. The prescribed condition at the upstream boundary is a sudden increase of pressure from zero to a constant value of 2 kPa (*Note*: numerically, the rise occurs in one grid length, namely 1 m in this instance). The dimensions of the ballast ($b = 8$ m, $h = 0{\cdot}5$ m) are typical for ballast track tunnels and the numerical values of its properties ($e = 0{\cdot}4$, $r = 10^{4{\cdot}5}$ Pa s/m^2) are taken to be indicative of an operational high-speed tunnel.

The distance scale in Figure 8 is chosen relative to axes moving at the ambient sonic speed, namely 340 m/s in all examples herein. In the absence of ballast or other dissipative influences, a step wavefront would propagate indefinitely far along the tunnel as a simple shock, travelling about 3 m/s faster than the chosen axes. In this example, however, a markedly different behaviour is observed. Initially, the leading part of the wavefront

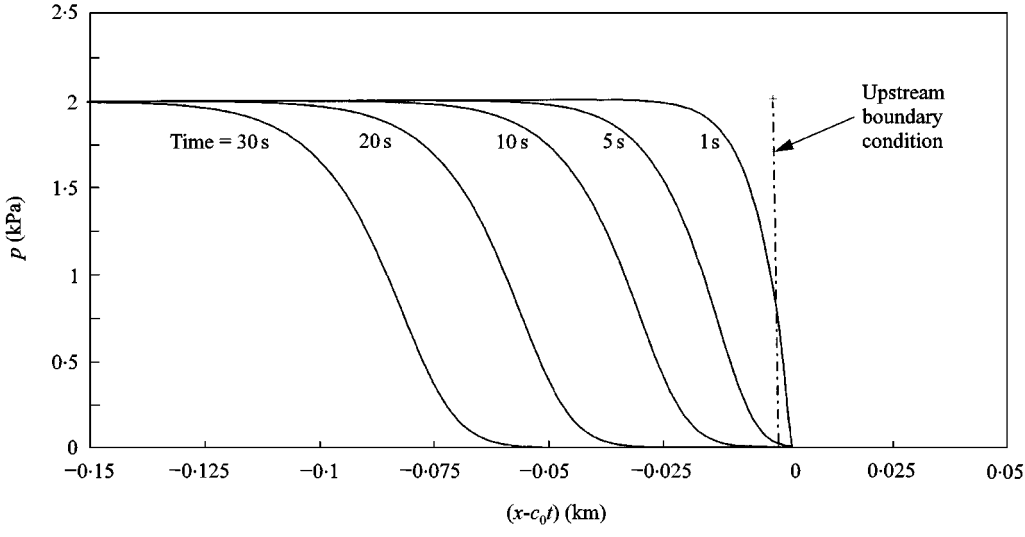

Figure 8. Evolution of a step wavefront ($b = 8$ m, $h = 0{\cdot}5$ m, $e = 0{\cdot}4$, $r = 10^{4{\cdot}5}$ Pa s/m^2).

propagates more rapidly than the ambient sound speed, but this tendency is soon overridden by the effects of the ballast.

The behaviour admits to a simple physical interpretation. Consider first the conditions at the leading step of the wavefront as it propagates along the tunnel. When the step reaches any particular location, it encounters ballast containing air at the same pressure as the undisturbed tunnel. As the impressed pressure increases, air begins to flow into the ballast, simultaneously increasing the pressure in the ballast and decreasing the pressure in the open tunnel. This process is repeated at each successive location encountered by the wavefront so the magnitude of its leading edge is continuously eroded.

Now consider conditions at some point on the wavefront behind the leading step. Conceptually, exactly the same process applies, but there is an important difference. When the chosen point reaches any particular position, it encounters ballast that has already been pressurized by earlier parts of the wave. As a consequence, the induced rate of flow is smaller than that which occurs close to the leading step and so the rate of erosion of pressure is also smaller. At sufficiently large distances behind the step, the rate is very small indeed.

After a short time, the wavefront settles down to a shape that is characteristic of its strength and of the tunnel in which it is propagating. Thereafter, the erosion process is repeated as the wavefront encounters each new section of ballast, but the effect is counterbalanced by inertial steepening and so the wavefront shape remains nearly constant. When successive large-time curves are shifted so that they superimpose upon one another, it is found that they are nearly identical. That is, the shape of the wavefront has become constant and the only measurable effect of the ballast is to reduce the speed of propagation along the tunnel. In this example, the bulk wave speed is about 4·5 m/s slower than the reference axes whereas a simple shock of the same amplitude would travel about 3 m/s faster than the axes.

4.2. RAMP WAVEFRONT

Figure 9 shows the corresponding pressure distributions when the prescribed pressure at the upstream boundary rises more gently from zero to a constant value of 2 kPa. With

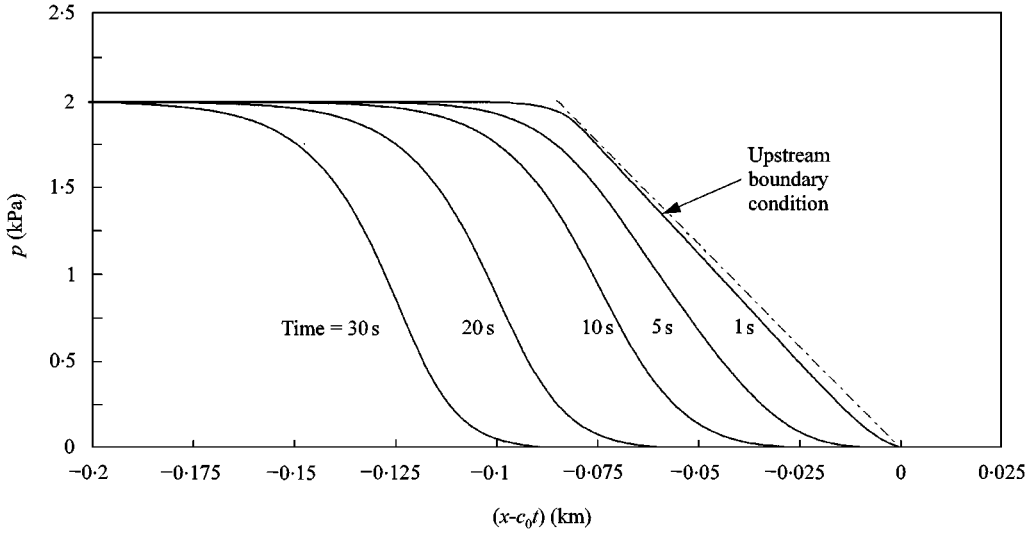

Figure 9. Evolution of a ramp wavefront ($b = 8$ m, $h = 0{\cdot}5$ m, $e = 0{\cdot}4$, $r = 10^{4{\cdot}5}$ Pa s/m^2)

a prescribed rate of change of 8 kPa/s, the length of the resulting ramp wavefront is approximately 85 m. This is indicative of a train entering an abrupt tunnel portal at about 250 km/h.

The dissipative influence of the ballast is exerted in a similar way to that observed for the step wavefront. The early time behaviour is less easy to see, however. This is partly because of the length of the ramp and partly because 0·25 s elapse before the whole wavefront enters the boundary. That is, the ballast is acting on the leading portions of the ramp before the later portions exist. The later-time behaviour is seen more easily; it bears a close resemblance to that shown in Figure 8 for a step wavefront.

In each of the pressure distributions in Figure 9, the maximum pressure gradient is greater than the prescribed initial value. That is, there has been net steepening of the wavefront even though the tunnel has a ballast track. Nevertheless, the ballast has prevented the development of the shock that would be expected after about 14 s in the absence of dissipative influences.

4.3. ASYMPTOTIC CONDITION

In the first of the above examples, a step wavefront becomes less steep as it propagates along the tunnel, but the process approaches an asymptotic condition after a few seconds. In the second example, a ramp wavefront becomes more steep and also approaches an asymptotic condition. Figure 10 confirms that both cases are approaching the same asymptote. That is, the steady state condition is independent of the initial pressure gradient. Furthermore, only short times are required to approach the asymptote quite closely (see section 4.4 for more detailed evidence). Nakao *et al.* [23] obtained qualitatively similar wavefronts in laboratory experiments.

These conclusions have important consequences for tunnel designers wishing to prevent the radiation of unacceptable micro-pressure waves from tunnel exit portals. First, modifications to tunnel *entrance* regions will have little influence on the outcome at *exit*

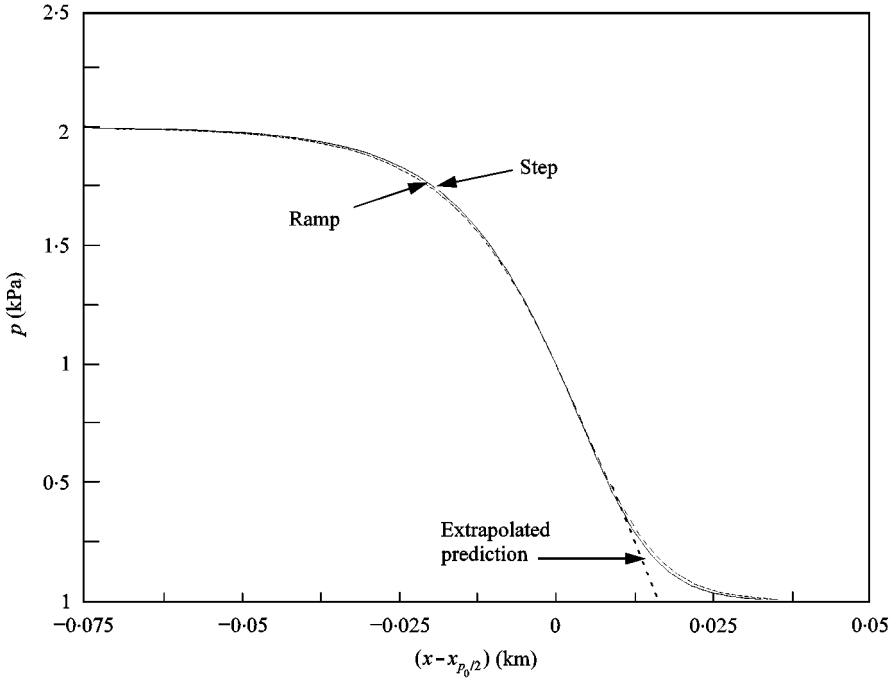

Figure 10. Asymptotic wavefront approached from above and below ($b = 8$ m, $h = 0{\cdot}5$ m, $e = 0{\cdot}4$, $r = 10^{4{\cdot}5}$ Pa s/m^2, $p_0 = 2$ kPa, $\dot{P}_0 = 8$ and 680 kPa/s, time = 70 s).

portals except in tunnels that are too short for the asymptotic condition to be approached. More important, if ballast is provided expressely for the purpose of preventing excessive micro-pressure waves, it should be concentrated in the region upstream of the exit portal, not distributed uniformly along the tunnel. In a long tunnel, this could represent a major cost saving.

4.4. TIME TO APPROACH ASYMPTOTIC CONDITION

Figure 11 shows the evolution of the maximum pressure gradients of various wavefronts as they propagate along the tunnel. In each case, the upstream pressure increases linearly from zero to 2 kPa and is then held constant. The curves denoted by initial gradients of 680 kPa/s and 8 kPa/s are deduced from the same data that was used to produce Figures 8 and 9. The other curves have been obtained by repeating the whole process using different initial pressure gradients. The implied lengths of the initial ramps range from 1 m (680 kPa/s) to 170 m (4 kPa/s). This figure is consistent with results given by Aoki *et al.* [24], who used Burger's equation to predict the asymptotic state of viscous shock waves.

The practical significance of this figure is that it can be used to estimate the length of ballast track that would be necessary to ensure that the wavefront arriving at the tunnel exit portal is dominated by the ballast. As an example, suppose that the target condition is within $\pm$ 25% of the asymptotic value. This is achieved for the step wavefront in a time of about 4 s and for the 8 kPa/s ramp in about 15 s, corresponding to ballast lengths of 1·4 km and 5·1 km respectively.

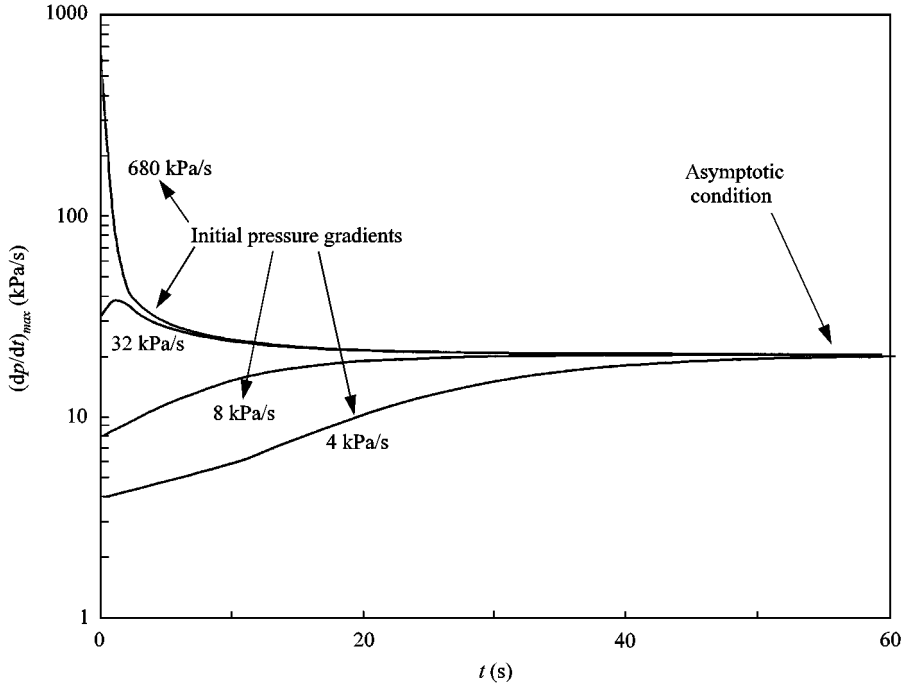

Figure 11. Evolution of maximum pressure gradients ($b = 8$ m, $h = 0{\cdot}5$ m, $e = 0{\cdot}4$, $r = 10^{4{\cdot}5}$ Pa s/m^2, $p_0 = 2$ kPa).

4.5. INFLUENCE OF PRESSURE AMPLITUDE

The particular asymptotic condition obtained above is applicable only for the chosen pressure amplitude of 2 kPa. When the analysis is repeated with smaller or greater amplitudes, different asymptotes are obtained. A close family resemblance is demonstrated in Figure 12, however, in which *both* axes are scaled by the incident pressure amplitude p_0. The maximum gradients of the four curves are nearly equal, showing that the pressure gradient varies approximately as the square of p_0. Thus, for example, if the asymptotic steepness of a 2 kPa wavefront is approximately 24 kPa/s, then the corresponding steepness of a 1 kPa wavefront will be about 6 kPa/s. For future use (see Appendix A), note that the asymptotic steepness of a 0·75 kPa wavefront with these ballast properties would be about 3·4 kPa/s.

Historically, it has been unusual for the amplitudes of individual wavefronts in railway tunnels to exceed about 2 kPa, but this might change as the use of aerodynamically sealed rolling stock becomes more widespread. There are strong commercial incentives to pursue this path because the limiting of pressure amplitudes is equivalent to limiting train speeds. Alternatively, in the case of new tunnels with prescribed speeds, it is equivalent to placing a lower limit on the permitted tunnel cross-sectional area.

Whether the pressure increase is caused by increased train speed or by decreased tunnel area, it will be accompanied by a decrease in time of development of the pressure rise during train entry. Therefore, the upstream pressure gradient will increase even more than the amplitude. Using Figure 11, the time required for the ballast to assert near-asymptotic conditions will usually decrease.

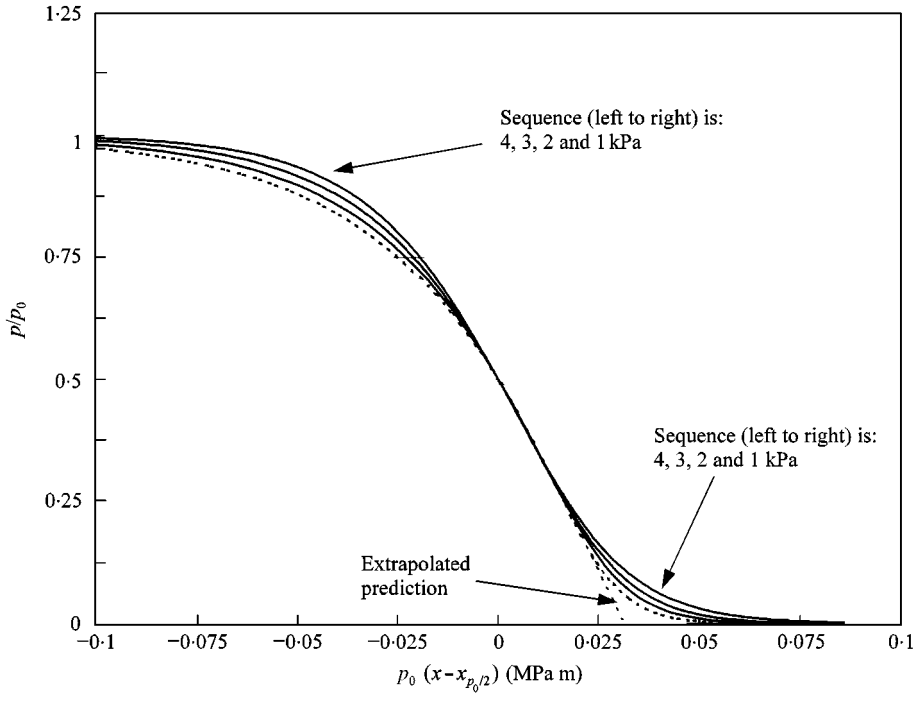

Figure 12. Influence of pressure amplitude on asymptotic wavefront shape ($b = 8$ m, $h = 0{\cdot}5$ m, $e = 0{\cdot}4$, $r = 10^{4{\cdot}5}$ Pa s/m^2).

5. SKIN FRICTION

The overall goal of the study within which the reported work has been undertaken is to develop reliable methods of predicting the evolution of wavefronts in real tunnels. To achieve this goal, it is necessary to consider the influence of skin friction as well as that of ballast. For the purposes of the present paper, however the inclusion of skin friction would reduce clarity. In particular, it would eliminate the possibility of developing the asymptotic states that are so crucial to understanding the influence of ballast.

One consequence of skin friction is that it gradually reduces the amplitudes of wavefronts as they propagate along a tunnel. Using Figure 12, we many deduce that the asymptotic steepnesses of the wavefronts will also reduce. If the ballasted region of tunnel is of sufficient length, the real wavefront should closely resemble a succession of asymptotic states with reducing amplitudes and reducing pressure gradients. This is consistent with measurements at full scale.

In principle, account should be taken of *unsteady* skin friction as well as quasi-steady skin friction. In the absence of ballast and other complications, unsteady skin friction is the only important phenomenon constraining the steepening of wavefronts in tunnels. Nevertheless, it is not sufficiently powerful to prevent the development of severe sonic booms in some slab track tunnels and so it cannot have a major impact on the asymptotic conditions predicted herein. Its primary influence in ballast track tunnels will be an additional contribution to the decay process attributed to quasi-steady skin friction in the preceding paragraph.

6. CONCLUSIONS

1. A numerical model of wave propagation in tunnels with ballast track has been developed for a simplified condition in which skin friction is neglected. The model enables the identification of behaviour that would be obscured if skin friction were included.
2. The most important properties of tunnel ballast are its porosity and resistivity. For a given porosity and depth of ballast, there exists a critical resistivity, above which non-oscillatory responses to impressed pressure changes are predicted. This state corresponds to behaviour observed in real tunnels.
3. For any particular uniform ballast, an asymptotic wavefront shape exists that is dependent only on the amplitude of the constant pressure region behind the wavefront.
4. The maximum pressure gradient in the asymptotic wavefront varies approximately as the square of wavefront amplitude.
5. The time required for a wavefront to approach the asymptotic state is sufficiently small to be of significance in tunnel design. In particular, ballast introduced solely for the purpose of reducing the radiation of micro-pressure waves from tunnel exit portals should be concentrated in the exit region of the tunnel.
6. In real tunnels, skin friction gradually erodes the amplitudes of wavefronts, but has little direct influence on their shapes. Wavefronts in real tunnels with ballast tracks may therefore approximate to a succession of inviscid asymptotic states.

ACKNOWLEDGMENTS

The authors are pleased to acknowledge a financial contribution towards early parts of this work from the TRANSAERO project in the European Commission's Brite Euram programme. They are also pleased to acknowledge support from The British Council for related collaboration with Japanese researchers.

REFERENCES

1. S. OZAWA, T. UCHIDA and T. MAEDA 1978 *Quarterly Report of the Railway Technical Research Institute* **19**, 77–83. Reduction of micro-pressure wave radiated from tunnel exit by hood at tunnel entrance.
2. K. TAKAYAMA, A. SASOH, O. ONODERA, R. KANEKO and Y. MATSUI 1995 *Shock Waves* **5**, 127–138. Experimental investigation on tunnel sonic boom.
3. R. GRÉGOIRE, J.-M. RETY, F. MASBERNAT, V. MORINIÈRE, M. BELLENOUE and T. KAGEYAMA 1997 *9th International Symposium on the Aerodynamics and Ventilation of Vehicle Tunnels, Aosta Italy*, BHR Group, 877–904. Experimental study (scale 1/70th) and numerical simulations of the generation of pressure waves and micro-pressure waves due to high speed train–tunnel entry.
4. S. OZAWA, K. MURATA and T. MAEDA 1997 *9th International Symposium on the Aerodynamics and Ventilation of Vehicle Tunnels, Aosta Italy, BHR Group*, 935–950. Effect of ballasted track on distortion of pressure wave in tunnel and emission of micro-pressure wave.
5. T. AOKI, Y. HARITA, Y. NOGUCHI, Y. NAKAGAWA, N. KONDOH and K. MATSUO 1991 *International Symposium on Active Control of Sound and Vibration*, 291–296. Investigations of active control of impulsive noise.
6. T. AOKI, A. E. VARDY and J. M. B. BROWN 1999 *Journal of Sound and Vibration* **220**, 921–940. Passive alleviation of micro-pressure waves from tunnel portals.
7. M. LIANG, T. KITAMURA, T. MAEDA, S. YAMADA, T. KOSAKA, K. MIYATA and S. YAMADA 1995 *Journal of Acoustical Society of Japan* (*E*) **16**, 363–368. Active attenuation of tunnel pressure wave with negative pressure gradient generated by positive pressure.
8. M. NISHIMURA, M. KONDO, K. IWAMOTO and Y. TSUJIMOTO 1994 *Inter-noise* '94, 1383–1388. Active attenuation of impulsive noise from a railway tunnel exit.

9. S. OZAWA 1984 *Japanese Railway Engineering* **24**, 2–5. Countermeasures to reduce booms from exits of Shinkansen tunnels.
10. K. KAGE, H. MIYAKE and S. KAWAGOE 1995 *JSME International Journal*, *Series B* **38**, 191–198. Numerical study of compression waves produced by high-speed trains entering a tunnel (effects of shape of hood).
11. T. MAEDA 1982 *Quarterly Report of the Railway Technical Research Institute Japan* **23**, 34–37. Reduction of micro pressure waves radiated from tunnel exit portal by branches in tunnel.
12. N. SUGIMOTO 1996 *Journal of the Acoustical Society of America* **99**, 1971–1976. Acoustical solitary waves in tunnels with an array of Helmholtz resonators.
13. T. OGAWA and K. FUJII 1997 *Computers and Fluids* **26**, 565–585. Numerical investigation of three-dimensional compressible flows induced by a train moving into a tunnel.
14. K. EHRENDORFER and H. SOCKEL 1997 *9th International Symposium on the Aerodynamics and Ventilation of Vehicle Tunnels*, *Aosta*, *Italy*, 863–876. The influence of measures near the portal of railway tunnels on the sonic boom.
15. S. MASHIMO, E. NAKATSU, T. AOKI and K. MATSUO 1996 *Transactions of the Japanese Society of Mechanical Engineers* **62**, 169–185. Attenuation and distortion of compression waves in a high speed railway tunnel.
16. T. FUKUDA, M. IIDA, T. MAEDA, K. NAKATANI, K. MAENO and H. HONMA 1997 *21st International Symposium on Shock Waves*, *Great Keppel Island*, *Australia*, 20–25 July, 755–760. Distortion of the compression wave during propagation in a high-speed railway tunnel.
17. P. M. MORSE 1939 *Journal of the Acoustical Society of America* **11**, 105–120. The transmission of sound inside pipes.
18. P. M. MORSE 1948 *Vibration and Sound*. New York: Mc-Graw-Hill.
19. S. OZAWA, T. MAEDA, T. MATSUMURA and K. UCHIDA 1993 *International Conference on Speedup Technology for Railway and Maglev Vehicles*, *Yokohama*, Vol. 2. 299–304. Effect of ballast on pressure wave propagation through tunnels.
20. T. F. W. EMBLETON, J. E. PIERCY and G. A. DAIGLE 1983 *Journal of the Acoustical Society of America* **74**, 1239–1244. Effective flow resistivity of ground surfaces determined by acoustical measurements.
21. E. B. WYLIE and V. L. STREETER 1993 *Fluid Transients in Systems*. Englewood Cliffs, Prentice-Hall.
22. R. S. BENSON and A. S. ÜCER 1971 *International Journal of Mechanical Science* **13**, 819–824. An approximate solution for non-steady flows in ducts with friction.
23. S. NAKAO, T. AOKI and K. MATSUO 1998 *4th KSME-JSME Fluids Engineering Conference* (*FEC4*), *Pusan*, *Korea*, 18–21 *October*.
24. T. AOKI, S. NAKAO, K. MATSUO, H. KASHIMURA and T. YASUNOBU 1997 *21st International Symposium on Shock Waves*, *Great Keppel Island*, *Australia*, 20–25 *July*, *paper* 1140. Attenuation and distortion of compression and shock waves propagating along high speed railway model tunnel.

APPENDIX A: COMPARISON WITH MEASURED DATA

Although many measurements exist of pressure histories in railway tunnels, very few have sufficient detail to enable the shapes of wavefronts to be observed. Of these, the only one known to the authors in a simple ballast track tunnel of adequate length is the 63 m^2 Rokko Tunnel in Japan [15]. Measurements from this paper have been reproduced in Figure 1 herein.

Figure A1(a) shows the measured pressure history 11 km from the entrance portal. After travelling so far along the tunnel, the amplitude of the wavefront has been greatly attenuated by skin friction. It would therefore not be appropriate to compare it with the asymptotic form of a wavefront with the same amplitude as the initial wavefront. Instead, the measured trace is compared with the predicted asymptotic shape of a wavefront with an amplitude indicative of the instantaneous condition, namely 0·75 kPa. The ballast is assumed to be 0·6 m deep, to have a porosity of 0·35 and an effective resistivity of 10^5 Pa s/m^2. These values lead to a smaller rate of change of pressure than that predicted in section 4·5 for a wavefront of equal magnitude in a different ballast. By inspection, the shapes of the measured and theoretical curves are broadly similar even though the latter is

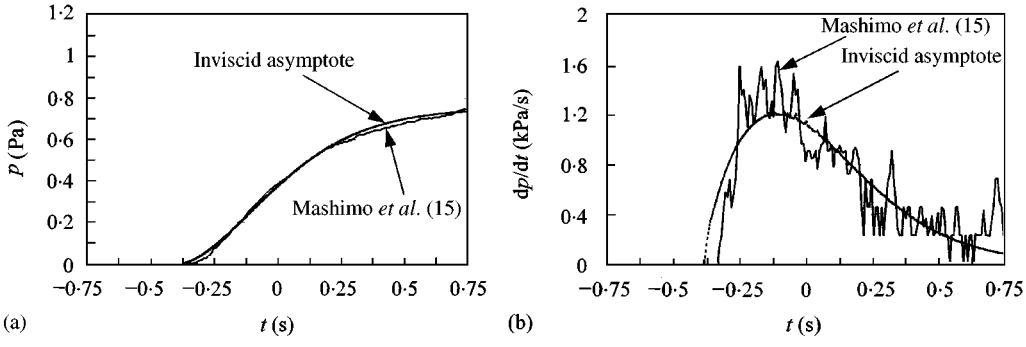

Figure A1. Comparison of measured data and predictions based on inviscid, asymptotic conditions ($b = 8$ m, $h = 0{\cdot}6$ m, $e = 0{\cdot}35$, $r = 10^5$ Pa s/m^2, $p_0 = 0{\cdot}75$ kPa). (a) pressure; (b) pressure gradients.

based on inviscid conditions.

Figure A1(b) shows rates of change of pressure close to the wavefront. This is a more severe test of the validity of the predicted shape than the simple comparison in Figure A1(a). When interpreting this Figure, three factors must be taken into account:

(1) The values chosen for the porosity, depth and effective resistivity of the ballast are believed to be realistic, but the true values for the particular tunnel are not known.
(2) The "measured" values of $\partial p/\partial t$ have been smoothed numerically to reduce the influence of noise in the raw data.
(3) The influence of numerical dissipation at the toe of the asymptotic curve has been restricted by curtailing the permitted length of the toe.

Given the unavoidable limitations of these comparisons, it would not be reasonable to conclude that Figure A1 validates the theoretical method. Neither is it sufficiently strong to confirm the hypothesis that the local shape of the asymptotic wavefront is nearly independent of skin friction. It is reasonable, however, to conclude that the comparisons are consistent with the theoretical trends and with predictions based on the hypothesis. In the absence of experimental evidence to the contrary, the authors propose to proceed with caution on the assumption that the methodology is sufficiently robust for engineering design purposes.

APPENDIX B: NOMENCLATURE

Scalars

a	cross-sectional area (m^2)
b	width of ballast track (m)
C	compliance of ballast per unit area (m/Pa)
c	speed of sound (m/s)
e	porosity of ballast
H	inertance of ballast (Pa s^2/m)
h	depth of ballast (m)
$\dot{P}$	prescribed rate of change of pressure (Pa/s)
p	static pressure in tunnel (Pa)
R	resistance of ballast per unit area (Pa s/m)
r	resistivity of ballast (Pa s/m^2)
s	Laplace transform parameter (1/s)
T	current time instant

T^*	time for which accelerations influence ballast response (s)
t	time (s)
t^*	time measured backwards from current instant (s)
u	mean velocity (m/s)
W	weighting function
w	vertical velocity in ballast (based on total area) (m/s)
x	distance along tunnel axis (m)
z	distance below ballast surface (m)
α	damping parameter (see equation (9))
β	damping parameter (see equation (18))
γ	ratio of principal specific heat capacities
ζ	displacement of air in the neck of a resonator (m)
ρ	mass density (kg/m^3)
ξ	apparent mass coefficient
ω_n	natural frequency (s^{-1})
$\mathscr{L}$	Laplace transform operator

Subscripts

0	initial condition, surface condition
A,B	solution points
crit	critical damping
k	arbitrary element in summation series
L	limiting condition (practical)
L,R	points on wave paths
$P_0/2$	mid-pressure position on wavefront
∞	reference condition, limiting condition (asymptote)

Superscripts

$'$	Laplace transformed